Baseband Superregenerative Amplification

Pere Palà-Schönwälder, *Member, IEEE*, F. Xavier Moncunill-Geniz, Jordi Bonet-Dalmau, *Member, IEEE*, Francisco del-Águila-López, and Rosa Giralt-Mas

***Abstract*—This paper describes a technique for exploiting circuit instability to achieve baseband linear amplification. The input signal is periodically sampled by a first-order unstable circuit, and amplification is achieved by the exponentially growing natural response. A low-pass sampled amplifier response is achieved. An operational amplifier implementation of the circuit is described, and the main practical limiting factors are presented. Several applications and experimental results are provided.**

***Index Terms*—Amplifiers, analog circuits, circuit stability, low power, superregenerative receiver.**

I. Introduction

LINEAR circuits are fundamental building blocks in analog signal processing. The response of a linear circuit may be written as the sum of two components: the natural response and the forced response. It is a well-known fact that the shape of the natural response only depends on the circuit and is independent of the input signal [1]. All of the natural poles in a stable circuit are located in the left half of the complex s-plane, which translates into a natural response that vanishes as $t \to \infty$. Circuit stability is usually required for a circuit to perform as an analog signal processor, because otherwise an exponentially growing term of the natural response would mask the desired forced response. From this, it follows that circuit instability is often considered to be an undesirable phenomenon and one that should be avoided.

To gain some insight into how an unstable system could perform a useful task, we can look to a very different field to the one considered herein. Consider an inverted pendulum (Fig. 1) : a rod is kept near the unstable upper equilibrium point for $t < 0$ and is released at $t = 0$. Even for a very small displacement from the equilibrium point, the rod soon deviates appreciably from the vertical line. In the absence of external perturbations, if the system is photographed after a fixed period of time t_G, the angular position of the rod in the photograph allows one to infer the exact angle at which the mass was released at $t = 0$. In this system, instability provides great amplification of the initial displacement.

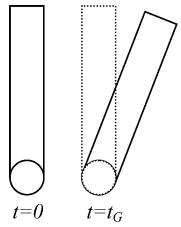

Fig. 1. Inverted pendulum example. Rod slightly apart from the equilibrium position at $t = 0$ and at the instant $t = t_G$.

Regenerative comparators [2] may be interpreted in a qualitatively similar way to the system described: they take advantage of the instability that results from positive feedback to achieve fast switching. Regenerative comparators have proven to be the optimum choice in switching time versus low power consumption [2], [3].

Superregenerative receivers [4] are another class of circuits in which instability plays a major role. This class of receiver consists of a variable gain amplifier that is fed back by a bandpass filter. The variable gain allows making the overall system stable or unstable, i.e., exhibiting decaying or raising oscillations, depending on a periodic external quench signal. Analyzing a superregenerative receiver in the so-called linear mode of operation shows that the peak amplitude of the generated RF pulses is dependent on the amplitude of an RF input signal injected into the receiver at certain time intervals [4]–[6]. In these receivers, the exponentially growing response during the unstable intervals allows one to achieve a significant amplification factor with remarkably low power consumption. As in the example of the inverted pendulum, higher amplification is achieved by giving the system more time to operate in the unstable region.

In Section II, this paper describes a baseband implementation of a superregenerative receiver proposing a simple first-order circuit in which samples of an input signal are periodically amplified by the exponentially growing natural response of an unstable circuit [7]. Implementation-specific details on using an operational amplifier (OA) as the active element are given in Section III, whereas Section IV is devoted to describing several applications and experimental results of the proposed approach, including a low-power linear amplifier, a variable-gain amplifier, a logarithmic amplifier, and a mixer. Concluding remarks are provided in Section V.

II. Basic Operation

Consider the basic circuit diagram depicted in Fig. 2, in which the ideal switch is opened at $t = 0$.

Manuscript received April 17, 2008; revised August 27, 2008. First published December 02, 2008; current version published September 02, 2009. This work was supported by the Spanish Dirección General de Investigación under Grant TEC2006-12687/TCM. This paper was recommended by Associate Editor S. Mirabbasi.

P. Palà-Schönwälder, J. Bonet-Dalmau, F. del-Águila-López, and R. Giralt-Mas are with the Department of Signal Theory and Communications (TSC), School of Engineering of Manresa (EPSEM), Universitat Politècnica de Catalunya (UPC), 08242 Manresa, Spain (e-mail: pere.pala@upc.edu).

F. Xavier Moncunill-Geniz is with the Department of Signal Theory and Communications (TSC), School of Engineering of Manresa (EPSEM), Universitat Politècnica de Catalunya (UPC), 08242 Manresa, Spain, and also with the School of Telecommunications Engineering of Barcelona, Universitat Politècnica de Catalunya (UPC), 08034 Barcelona, Spain.

Digital Object Identifier 10.1109/TCSI.2008.2010153

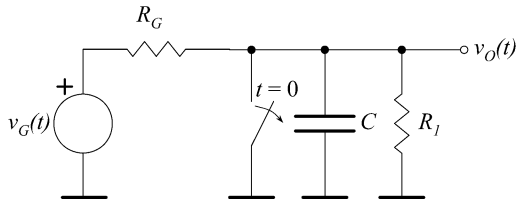

Fig. 2. Basic circuit.

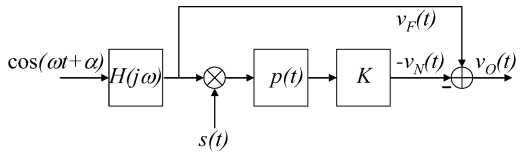

Fig. 3. Equivalent block diagram.

Straightforward analysis in the Laplace domain [7] shows that the transfer function

$$H(s) = \frac{V_O(s)}{V_G(s)} \tag{1}$$

is given by

$$H(s) = \frac{1}{R_G C}\frac{1}{s + \frac{1}{RC}} \tag{2}$$

with

$$R = \frac{R_1 R_G}{R_1 + R_G}. \tag{3}$$

The circuit response to an input

$$v_G(t) = \cos(\omega t + \alpha) \tag{4}$$

may be written as

$$v_O(t) = v_N(t) + v_F(t) \tag{5}$$

where, defining

$$A = |H(j\omega)| \tag{6}$$

$$\varphi = \arg(H(j\omega)) \tag{7}$$

the natural and the forced responses are, respectively, given by

$$v_N(t) = -A\cos(\alpha + \varphi)\exp\left(\frac{-t}{RC}\right)u(t) \tag{8}$$

$$v_F(t) = A\cos(\omega t + \alpha + \varphi)u(t). \tag{9}$$

Assuming that R_G is positive, the product *RC* may become negative if $C < 0$ or $-R_G < R_1 < 0$. If either of these conditions holds, the transfer function (2) has a pole in the right-hand plane and the circuit is said to be unstable. In this case, we may define the positive time constant of the natural response as

$$\tau = -RC. \tag{10}$$

As t increases up to an instant t_G, the natural response $v_N(t)$ soon becomes the dominant term in $v_O(t)$, provided that the active devices remain in the linear range of operation.

The response of the circuit in Fig. 2 for $0 < t < t_G$ may also be viewed in terms of the equivalent system depicted in Fig. 3.

The block labeled as $H(j\omega)$ is a low-pass filter with a transfer function given by (2) and taking $s = j\omega$. Despite being unstable, this equivalent filter is assumed to give the response

$$A\cos(\omega t + \alpha + \varphi) \tag{11}$$

to the input shown. The sampling function $s(t)$ is a Dirac impulse

$$s(t) = \delta(t) \tag{12}$$

the pulse-shaping block labeled $p(t)$ is a linear time-invariant system characterized by a normalized impulse response

$$h(t) = p(t) \tag{13}$$

exhibiting a maximum value of unity, i.e.,

$$p(t) = \begin{cases} \exp\left(\frac{t-t_G}{\tau}\right), & 0 < t \le t_G \\ 0, & \text{otherwise} \end{cases} \tag{14}$$

and the amplification factor K is given by

$$K = \exp\left(\frac{t_G}{\tau}\right). \tag{15}$$

If the forced response can be neglected, it follows that the observed response is an exponentially growing pulse whose final amplitude at $t = t_G$ is proportional to that of the sample of $v_G(t)$ at $t = 0$ by a factor K that may become extremely large.

Now, if the switch in Fig. 2 is closed at $t = t_G$ and opened at the next sampling instant $t = t_S$, the preceding analysis is still valid if a new time origin, $t' = t - t_S$ is taken. Periodically, repeating the procedure gives a response composed of exponentially growing pulses each conveying a sample of $v_G(t)$. During the time intervals in which the switch is open, this output is also the response of the system in Fig. 3, taking the sampling function as

$$s(t) = \sum_{k=-\infty}^{\infty} \delta(t - kt_S). \tag{16}$$

Now, since the circuit is linear, this result may be applied to any signal that can be written as a linear combination of signals of the type (4), i.e., any signal for which the Fourier transform exists.

An outline of the resulting waveform for a sinusoidal input signal is depicted in Fig. 4.

III. Implementation

There are several options for implementing a circuit that behaves like the circuit depicted in Fig. 2. Next, we will address the implementation of a negative resistance based on the negative immittance converter principle depicted in Fig. 5, [8]. Balanced implementations based on cross-coupled transistors, such as those described in [9], are also possible and may be the best option for higher frequencies.

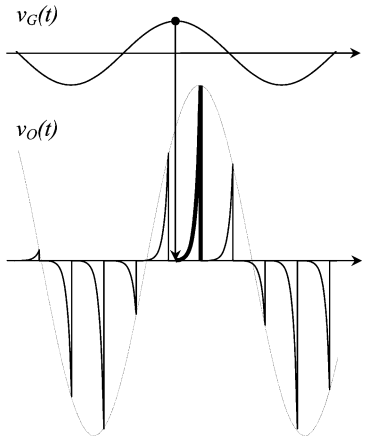

Fig. 4. Typical waveforms for a sinusoidal input signal. The dashed line represents the envelope of the pulses. Signals are not to scale, i.e., $v_O(t)$ is typically several orders of magnitude greater than $v_G(t)$.

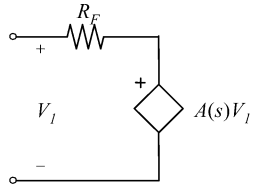

Fig. 5. Negative resistance implemented with a voltage-controlled voltage source.

The voltage-controlled voltage source in Fig. 5 may correspond to an OA-based noninverting amplifier. Straightforward analysis of the circuit in Fig. 5 shows that the input impedance is given by

$$Z_{\text{in}}(s) = \frac{R_F}{1 - A(s)} \tag{17}$$

which results in a negative resistor if $A(s) = A_O > 1$. For instance, if $A(s) = 2$, then $Z_{\text{in}} = -R_F$.

A. Amplifier Bandwidth

To evaluate the bandwidth requirement on $A(s)$, we may first compute the Fourier transform of $p(t)$,

$$P(f) = \frac{\exp(-j2\pi f t_G) - \exp(-t_G/\tau)}{(1/\tau) - j2\pi f}. \tag{18}$$

If $K \gg 1$, the real exponential in the numerator of (18) may be neglected, so that the bandwidth of $p\,(t)$ may be approximated by

$$\omega_{P(-3\,\text{dB})} = \frac{1}{\tau}. \tag{19}$$

Now, if we consider the common case in which $A(s)$ has a dominant pole, i.e.,

$$A(s) = \frac{A_0}{(s/p) + 1} \tag{20}$$

the input impedance (17) results in

$$Z_{\text{in}} = \frac{R_F}{1 - A_0} \frac{(s/p) + 1}{s/p(1 - A_0) + 1} \tag{21}$$

which has an equivalent circuit, as depicted in Fig. 6 with

$$R_1 = \frac{R_F}{(1 - A_0)} \tag{22}$$

$$R_A = \frac{R_F}{A_0} \tag{23}$$

$$C_A = \frac{A_0}{(pR_F)}. \tag{24}$$

To analyze the influence of the pole of $A(s)$ or, equivalently, that of the R_AC_A series combination on the overall circuit (Fig. 2) behavior, we may compute the resulting response to an input $\exp(j\omega t)u(t)$, which results in

$$v_O(t) = (A_1 \exp(p_1 t) + A_2 \exp(p_2 t) + A_F \exp(j\omega t))u(t) \tag{25}$$

where the poles are given by

$$p_1 = -\frac{1}{2}(p + p_E + p_A + \sigma) \tag{26}$$

$$p_2 = -\frac{1}{2}(p + p_E + p_A - \sigma) \tag{27}$$

and the corresponding residues are

$$A_1 = p_B \frac{(p_1 + p)}{(p_1 - p_2)(p_1 - j\omega)} \tag{28}$$

$$A_2 = p_B \frac{(p_2 + p)}{(p_2 - p_1)(p_2 - j\omega)} \tag{29}$$

$$A_F = p_B \frac{p + j\omega}{(p_1 - j\omega)(p_2 - j\omega)} \tag{30}$$

with

$$p_B = \frac{1}{R_G C} \tag{31}$$

$$p_A = \frac{1}{R_A C} \tag{32}$$

$$p_E = \frac{1}{RC} \tag{33}$$

$$\sigma = \sqrt{(p_A + p_E + p)^2 - 4pp_E}. \tag{34}$$

Note that, if p is sufficiently large, p_1, which is associated with an exponentially decaying term, may be approximated by

$$p_1 \approx -p \tag{35}$$

while the dominant, unstable pole p_2 may be approximated by

$$p_2 \approx -p_E = -1/RC \tag{36}$$

as in the ideal case. This result may be obtained rewriting (34) as

$$\sigma = (p_A + p_E + p)\sqrt{1 - \frac{4pp_E}{(p_A + p_E + p)^2}} \tag{37}$$

and making use of

$$\sqrt{1 - \varepsilon} \approx 1 - \varepsilon/2 \tag{38}$$

which holds for small ε.

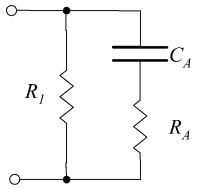

Fig. 6. Equivalent circuit of the negative impedance.

In the general case, the dominant residue A_2 depends on the input signal frequency and the particular circuit element values. From (29), it is clear that A_2 exhibits a first-order low-pass response with a -3-dB cutoff frequency

$$\omega_C = p_2 \tag{39}$$

which may be used as an estimate of the equivalent system's bandwidth and a low-frequency amplification given by

$$A_L = \frac{p_B(p_2+p)}{p_2(p_2-p_1)}. \tag{40}$$

As a result, the effect of the pole p in $A(s)$ is to add an exponentially decaying response term related to p_1, which may be neglected, and to change the time constant of the exponentially growing term, related to p_2. Hence, the results from Section II may still be applied taking the time constant

$$\tau = \frac{1}{p_2}. \tag{41}$$

Similarly, if we are only interested in the natural response, the equivalent system depicted in Fig. 3 is still valid if we substitute

$$H(j\omega) = -A_2(j\omega) \tag{42}$$

and dropping the path corresponding to the forced response.

B. Slew Rate and Switch on Resistance

When the switch is in the OFF-state, the amplifier slew rate (SR) limits the maximum amplitude that may be achieved for a given time constant τ. Specifically, if the amplifier output has to exhibit an exponential response given by

$$A_{\rm MAX}\exp\left(\frac{(t-t_G)}{\tau}\right) \tag{43}$$

which achieves an amplitude $A_{\rm MAX}$ at $t=t_G$, it is required that

$$\mathrm{SR} \geq \frac{|A_{\rm MAX}|}{\tau} \tag{44}$$

to preserve the exponential shape.

Also, for the switch to effectively discharge the capacitor between $t_G < t < t_S$, it is necessary that

$$\mathrm{SR} \geq \frac{|A_{\rm MAX}|}{(t_S-t_G)} \tag{45}$$

assuming that the switch ON resistance can be neglected.

If this is not the case, the switch-ON resistance $R_{\rm ON}$ must be sufficiently small to allow discharging C to a sufficiently negligible value. To ensure more than L dB attenuation, this means that

$$t_S - t_G > \frac{A_{\rm MAX}}{\mathrm{SR}} + \tau_{\rm ON}\left(0.115L\ln\left(\mathrm{SR}\frac{\tau_{\rm ON}}{A_{\rm MAX}}\right)-1\right) \tag{46}$$

where

$$\tau_{\rm ON} \approx R_{\rm ON}C. \tag{47}$$

IV. Applications and Results

A. Low-Power Linear Amplifier

The technique described allows exponentially growing pulses to be generated, providing samples of an amplified version of the input signal. For a given sampling frequency $f_S = 1/t_S$, increasing t_G/τ allows high gain to be achieved in a single stage, and this may reduce overall power consumption as a result.

In this case, it is worth pointing out that the resulting gain times bandwidth product may be higher than the gain-bandwidth product of the OA (GB_O) that implements the negative resistance. This is explained by the fact that, despite of the high amplification achieved by the circuit, the OA actually works in a low gain (typically 2) configuration.

Consider an input signal of bandwidth B, which is sampled at a frequency $f_S = kB$, with $k > 2$. From (15), the gain, expressed in decibels (dB)

$$G(\mathrm{dB}) = 20\log K \tag{48}$$

is given by

$$G(\mathrm{dB}) = 8.7\left(\frac{t_G}{\tau}\right). \tag{49}$$

Now, if we consider t_G to be a fraction of the sampling period, i.e.,

$$\delta = \frac{t_G}{t_S} \tag{50}$$

we may write

$$G(\mathrm{dB})B = \frac{8.7\delta}{(k\tau)} \tag{51}$$

where G is given in dB. Since δ and k are constants, and τ is an intrinsic parameter of the given amplifier configuration, it follows that the product $G(\mathrm{dB})B$ in (51) is a constant. Thus, halving the signal bandwidth allows the achievable gain (in dB) to be doubled. From this, it follows that, for sufficiently small B, the linear *GB* product eventually becomes larger than GB_O. This may allow the total number of stages required to achieve a prescribed gain to be reduced.

If the objective is to fully reconstruct an amplified version of the input signal, a sample-and-hold stage followed by a suitable low-pass filter may be added. Fig. 7(a) shows an implementation of the resulting system, excluding the final low-pass filter, and Fig. 7(b) shows the switch control waveforms. Note

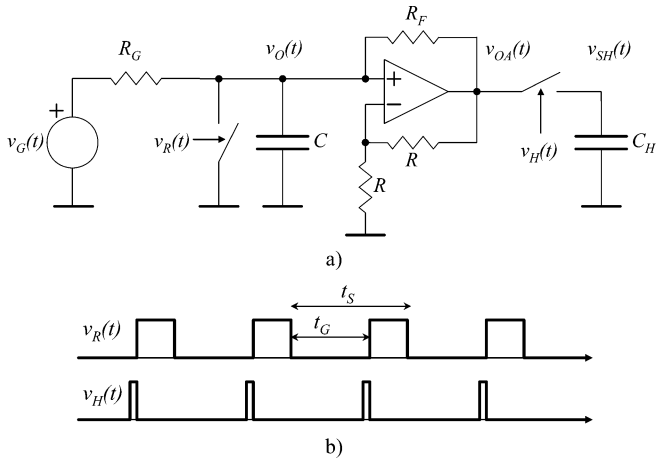

Fig. 7. Proposed amplifier structure. (a) Circuit diagram. (b) Control waveforms.

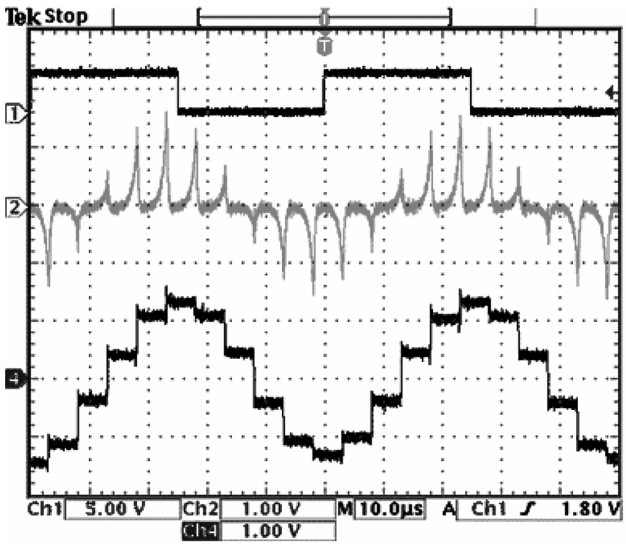

Fig. 8. Typical waveforms. Upper trace: signal synchronized to the 2-mVpp sinusoidal input. Middle trace: $v_{\rm OA}(t)$. Bottom trace $v_{\rm SH}(t)$.

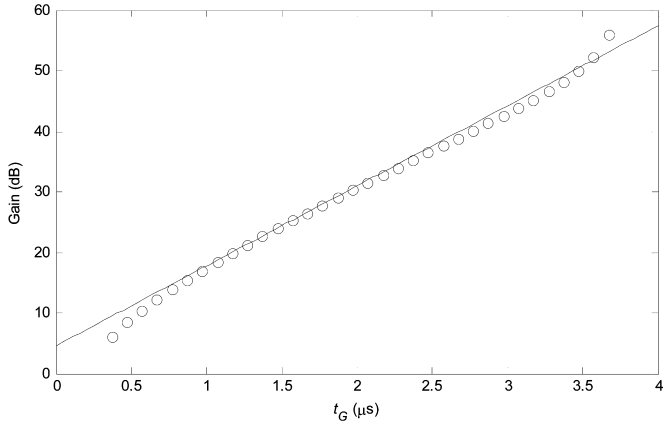

Fig. 9. Predicted (solid line) and measured gain (o) as a function of t_G.

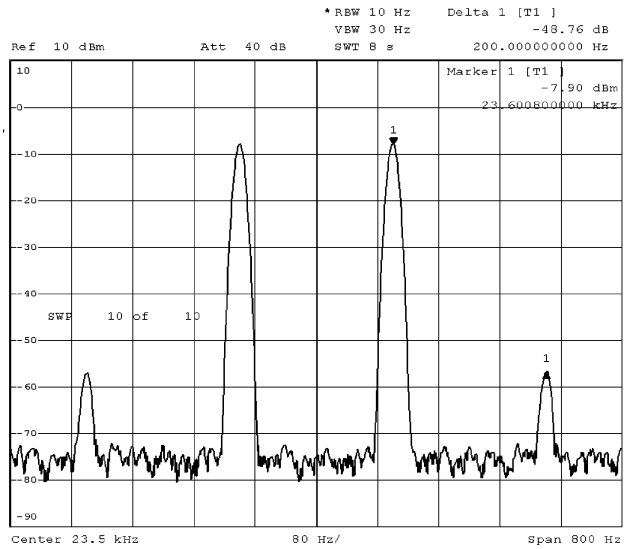

Fig. 10. Linearity test with a two-tone input. Input signal levels are -50 dBm.

that this design provides an added benefit as the OA output provides an additional x2 amplification while providing a low impedance node. In our implementation, a general purpose TL081CN OA (powered from $+5$ and -5 V rails) and conventional HEF4066BP CMOS switches were used. Nominal values of the other relevant components were $R_F = 470\ \Omega, R = 1.2$ k$\Omega, R_G = 1$ k$\Omega + 50\ \Omega$, and $C = 470$ pF. The circuit depicted is robust and only needs the usual offset compensation circuitry, which is not shown in Fig. 7(a) for the sake of clarity.

Fig. 8 depicts typical waveforms that may be achieved in practice. Further experimental waveforms and results for this circuit are described in [7]. It is also worth noting that the gain discrepancies observed in [7] are now explained by the results from Section III-A, which take the pole of the OA into account. For instance, taking $GB_O = 4$ MHz (typical for a TL081 OA) into the circuit in [Fig. 7(a)] with the mentioned component values gives $p_2 = 1.5 \times 10^6\ {\rm s}^{-1}$. Neglecting the pole of the OA would give $p_{2\rm IDEAL} = 2.5 \times 10^6\ {\rm s}^{-1}$. In [7], an experimental value of $\tau = 700$ ns was measured, which is in much better agreement with $1/p_2 = 660$ ns than with $1/p_{2\rm IDEAL} = 400$ ns.

The experimental gain versus t_G for a 1-kHz sinusoidal input signal sampled at $f_S = 200$ kHz is plotted in Fig. 9. This figure also shows the predicted gain due to the natural response—taking the results from Section III-A into account—with the nominal circuit element values given earlier. For low values of t_G the *forced* response cannot be neglected while, for sufficiently high values of t_G, *hangover* from the previous cycle [meaning that (46) is not met] translates into a gain higher than predicted.

The linearity of the resulting amplifier is mainly determined by saturation of the OA. This has been investigated on a 42-dB amplifier configuration using an input signal consisting of two tones at 23.4 and 23.6 kHz. For an input signal level of -50 dBm, the measured responses at 23.4 and 23.6 kHz were at -7.9 dBm, and the main intermodulation products at 23.2 and 23.8 kHz were at -58.2 dBm, as shown in Fig. 10. This was achieved with $f_s = 180$ kHz and $\delta = 0.5$.

From the circuit operation principle, it is clear that clock jitter may have a strong influence on the circuit's behavior. For instance, if we consider that t_G exhibits a Gaussian distribution

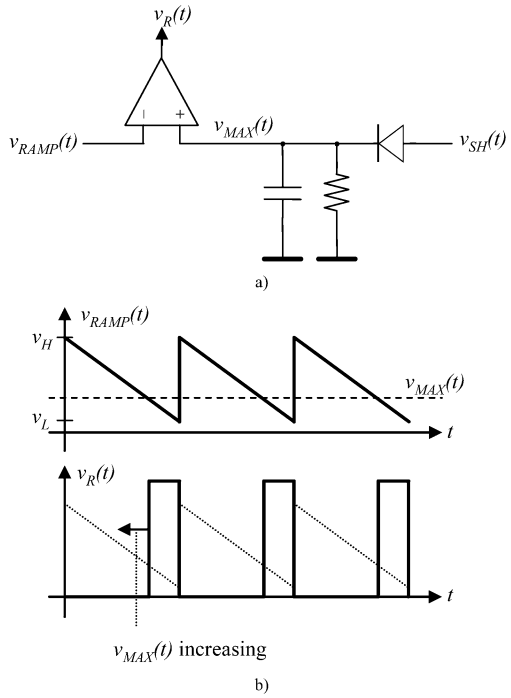

Fig. 11. (a) Block diagram of an automatic gain control loop. (b) Associated waveforms.

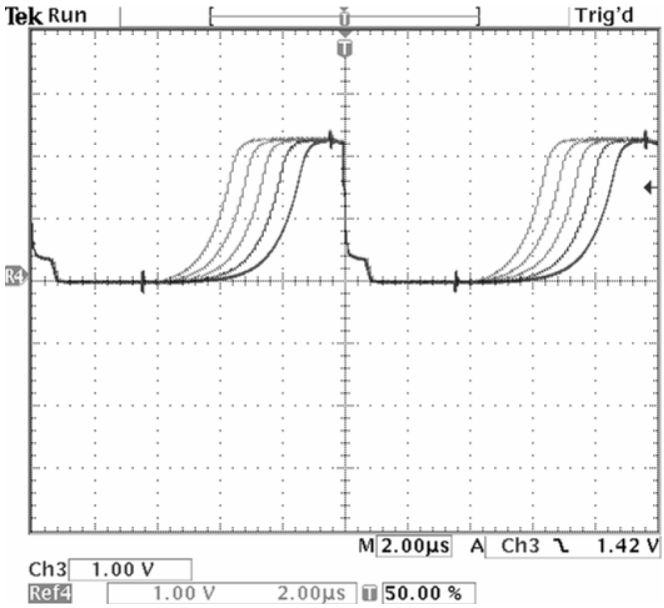

Fig. 12. Operation as a logarithmic amplifier. Output waveforms for a constant input of 160 (widest pulse), 80, 40, 20, and 10 mV (narrowest pulse).

around a nominal value, this translates into output samples that exhibit a lognormal (exponential of a Gaussian) amplitude distribution. However, if the jitter is small compared to the nominal value of t_G, the output amplitude distribution may also be adequately approximated by a Gaussian distribution. In any case, clock jitter translates into increased noise.

To investigate this effect on the same 42 dB amplifier configuration as described earlier, we programmed an Agilent 33250A signal generator to provide a 180-kHz-clock whose frequency was internally frequency modulated with noise [10]. When the frequency deviation was 18 kHz (10% of the nominal frequency), the displayed noise floor rose to -57 dBm, measured with a 10-Hz resolution bandwidth. However, for 1.8-kHz-frequency deviation (1% of the nominal frequency) the noise floor of -72 dBm was already very near to the -75-dBm noise-floor level, which was observed without any artificial modulation. In this case, it turns out that clock jitter may be neglected for any clock with reasonable jitter specifications.

B. Variable Gain Amplifier and Automatic Gain Control

The described circuit lends itself as a variable gain amplifier. For a fixed sampling frequency f_S, the gain G (in dB) may be linearly controlled by the duty cycle δ [7] as may be seen from Fig. 9, taking the new x-axis variable $\delta = t_G/5\ \mu$s.

Automatic gain control may be easily achieved with a suitable feedback loop controlling the duty cycle δ, as is sketched in the block diagram in Fig. 11. The switch control waveform $v_R(t)$ is obtained from a sawtooth signal of frequency f_S and the amplitude of the output signal. If the output signal amplitude increases, the duty cycle δ is decreased and vice versa.

Experimental results (using a 1N4148 diode and a comparator block built with a TL081 OA followed by a CMOS gate) show that the automatic gain control loop is able to compress a 40-dB input dynamic range into a 5-dB output dynamic range when $v_H = 1$ V and $v_L = -0.5$ V. In this case, the loop is able to synchronize for any input signal. Choosing $v_H = 0.9$ V and $v_L = 0.3$ allows the loop to track the same 40-dB input range without any significant change (less than 0.2 dB) in output amplitude. However, in this case, the loop needs an acquisition aid, e.g., in the form of a slow ramp increasing v_L from -0.5 to 0.3 V.

C. Logarithmic Amplifier

For sufficiently high gain, the OA goes into saturation, which is undesirable for linear operation. However, this may lead to another useful operating mode, which is described next.

The time it takes for an exponentially growing signal to achieve saturation V_{SAT},

$$v_i \exp(t/\tau) = V_{\mathrm{SAT}} \tag{52}$$

depends logarithmically on the initial amplitude v_i

$$t_{\mathrm{SAT}} = \tau(\ln V_{\mathrm{SAT}} - \ln v_i). \tag{53}$$

As a result, if the output reaches saturation in each sampling period, the output may be viewed as a pulsewidth-modulated signal whose average value is dependent on $\ln v_i$.

Fig. 12 depicts the measured $v_O(t)$ for different constant input signals showing a linear increase in the pulsewidth as the input signal amplitude is doubled. The circuit values were the same, as described in Section IV-A with $t_S = 10\ \mu$s and $t_G = 6\ \mu$s. The small pulse after the falling edge of $v_O(t)$ is due to the finite ON resistance of the switch and the finite saturation recovery time of the OA. Both may be optimized with commercially available parts. Also, a clamping circuit that avoids relying on the direct saturation of the OA would enhance

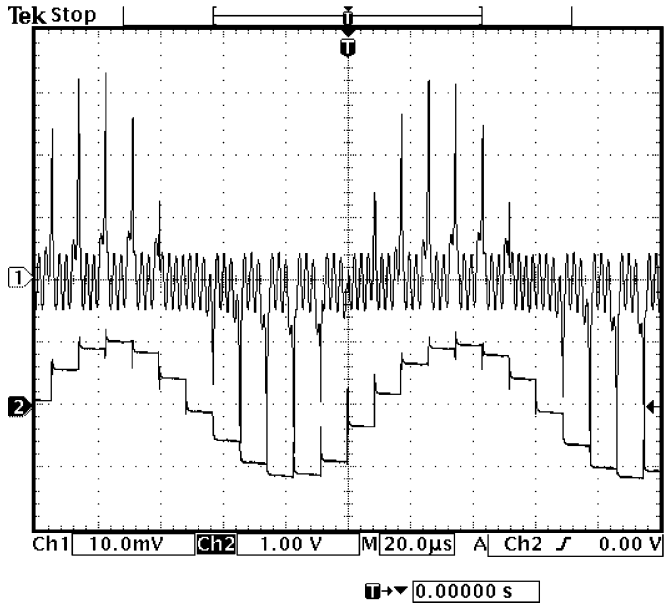

Fig. 13. Operation as a downconverting mixer for a 455-kHz sinusoidal input signal. Upper trace: signal measured at the generator output (V_{GO} in Fig. 14). Lower trace: sample-and-hold output of the downconverted 9-kHz signal.

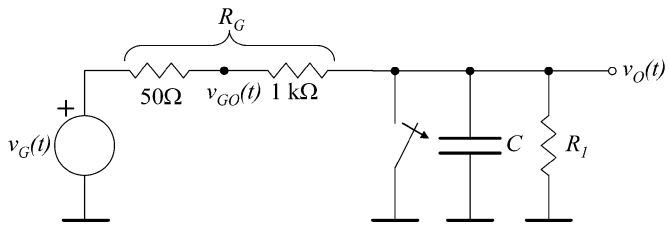

Fig. 14. Definition of $V_{GO}(t)$.

the saturation recovery time of the circuit. More idealized waveforms may be obtained including a final comparator to sharpen up the resulting waveform.

Note that in this configuration, the circuit behavior is similar to the logarithmic mode of operation in superregenerative receivers [6].

D. Downconverting Mixer

The sampling frequency may also be lower than that of the input signal if the latter is a bandpass signal. For instance, the circuit described (Fig. 7) may be used to downconvert a modulated signal centered around an intermediate frequency of 455 kHz. In this case, a sampling rate of 455/4 kHz may be used. Such a low sampling rate allows the circuit depicted in Fig. 7 to achieve sufficient gain.

As an example, Fig. 13 depicts the waveforms measured in an implementation of the circuit in Fig. 7 for a 455-kHz input signal with the sampling frequency adjusted to 116 kHz. The upper trace corresponds to the signal measured at the source terminals, i.e., v_{GO} in Fig. 14, *after* the internal 50 Ω resistor. This signal is a linear superposition of the sinusoidal input $v_G(t)$ and the circuit response $v_O(t)$. The exponentially growing pulses generated during the unstable periods are clearly visible. The bottom trace depicts the sample-and-hold output v_{SH} corresponding to the downconverted sinusoidal signal whose frequency is given by

$$f_{\mathrm{MIX}} = |455 - 4 \cdot 116| = 9 \quad [\mathrm{kHz}]. \tag{54}$$

In this configuration, $\delta = 0.5$ and the circuit achieves a conversion gain of 46 dB.

V. Conclusion

This paper describes a technique that makes use of the periodic instability of a first-order circuit to achieve sampled amplification. The approach may be viewed as a baseband implementation of the principle underlying the operation of the superregenerative receivers.

A block diagram equivalent to the operation of the circuit has been proposed. An OA-based implementation of the circuit has been described, taking into account the main factors that may limit the performance of the circuit.

Several applications with experimental results have been described. A broadband amplifier has been implemented, which, in contrast to conventional structures, is able to achieve a gain-bandwidth product greater than the gain-bandwidth product of the OA. The linearity and the sensitivity to clock phase jitter of this amplifier have been investigated. A variable gain amplifier and an automatic gain control loop have been implemented together with a pulsewidth-modulated logarithmic amplifier. Finally, the equivalent sampling performed by the circuit has been used to implement a downconverting mixer from 455 kHz to dc. Simulated and experimental results match the expected circuit behavior.

References

[1] R. E. Thomas and A. J. Rosa, *The Analysis and Design of Linear Circuits*. London, U.K.: Prentice-Hall, 1994.
[2] P. J. Lim and B. A. Wooley, "An 8-bit 200-MHz BiCMOS comparator," *IEEE J. Solid-State Circuits*, vol. 25, no. 1, pp. 192–199, Feb. 1990.
[3] P. Sunghyun and M. P. Flynn, "A regenerative comparator structure with integrated inductors," *IEEE Trans. Circuits Syst. I, Reg. Papers*, vol. 53, no. 8, pp. 1704–1711, Aug. 2006.
[4] E. H. Armstrong, "Some recent developments of regenerative circuits," in *Proc. IRE*, Aug. 1922, vol. 10, pp. 244–260.
[5] J. R. Whitehead, *Super-Regenerative Receivers*. Cambridge, U.K.: Cambridge Univ. Press, 1950.
[6] F. Xavier Moncunill-Geniz, P. Pala-Schonwalder, and O. Mas-Casals, "A generic approach to the theory of superregenerative reception," *IEEE Trans. Circuits Syst. I, Reg. Papers*, vol. 52, no. 1, pp. 54–70, Jan. 2005.
[7] P. Pala-Schonwalder, J. Bonet-Dalmau, F. X. Moncunill-Geniz, F. del Aguila-Lopez, and R. Giralt-Mas, "Exploiting circuit instability to achieve wideband linear amplification," in *Proc. IEEE ISCAS*, 2006, pp. 1401–1404.
[8] K. Soundararajan and K. Ramakrishna, "Nonideal negative resistors and capacitors using an operational amplifier," *IEEE Trans. Circuits Syst.*, vol. 22, no. 9, pp. 760–763, Sept. 1975.
[9] B. Jung and R. Harjani, "High-frequency LC VCO design using capacitive degeneration," *IEEE J. Solid-State Circuits*, vol. 39, no. 12, pp. 2359–2370, Dec. 2004.
[10] Agilent Technologies, "Agilent 33250A 80 MHz Function/Arbitrary Waveform Generator User's Guide," Mar. 2003 [Online]. Available: http://cp.literature.agilent.com/litweb/pdf/33250-90002.pdf

Pere Palà-Schönwälder (S'88--M'05) received the Eng. Telecommun. and Ph.D. degrees from the Universitat Politècnica de Catalunya (UPC), Barcelona, Spain, in 1989 and 1994, respectively.

He is currently an Associate Professor at the Department of Signal Theory and Communications, Technical College of Manresa, Manresa, UPC, Manresa, Spain, where he has been teaching circuit theory, analog signal processing, communications electronics, and radio-frequency (RF) design since 1990. He has been the project leader of several government and industry-funded research projects. His current research interests include circuit theory, computer-aided circuit design, nonlinear circuits, and the design of RF communication circuits.

F. Xavier Moncunill-Geniz received the Eng. Telecommun. and Ph.D. degrees from the Universitat Politècnica de Catalunya (UPC), Barcelona, Spain, in 1992 and 2002, respectively.

He is currently an Assistant Professor at the Department of Signal Theory and Communications, School of Telecommunications Engineering of Barcelona, UPC, where he is currently involved in the field of circuit theory and analog electronics, and he is also with the School of Engineering of Manresa, UPC, Manresa, Spain. His current research interests include radio-frequency circuit design with a particular emphasis on the theory and implementation of new superregenerative receiver architectures.

Jordi Bonet-Dalmau (S'92--A'00--M'04) received the Eng. Telecommun. and Ph.D. degrees from the Universitat Politècnica de Catalunya (UPC), Barcelona, Spain, in 1995 and 1999, respectively.

He is currently an Associate Professor at the Department of Signal Theory and Communications, Technical College of Manresa, UPC, Manresa, Spain. His current research interests include steady-state and stability analysis of nonlinear and distributed circuits.

Francisco del-Águila-López received the Eng. Telecommun. and Ph.D. degrees from the Universitat Politècnica de Catalunya (UPC), Barcelona, Spain, in 1996 and 2003, respectively.

He is currently an Assistant Professor at the Department of Signal Theory and Communications, Technical College of Manresa, UPC, Manresa, Spain, where he has been teaching circuit theory, analog electronics, data transmission, and telematics since 1997. He has also been involved in several government and industry-funded research projects. His research research interests include switched circuits, nonlinear circuits, and radio-frequency communication circuits design.

Rosa Giralt-Mas received the Eng. Telecommun. degree from the Universitat Politècnica de Catalunya (UPC), Barcelona, Spain, in 1995.

From 1993 to 1997, she was a Telecommunications Consultant. She is currently an Assistant Professor with the Department of Signal Theory and Communications, Technical College of Manresa, UPC, Manresa, Spain, where she has been teaching circuit theory, telecommunication systems engineering and project management since 1997. She has also been involved in several government and industry-funded research projects. Her current research interests include communication systems and project management.